processes

MDPI

Article

Improving Photocatalytic Hydrogen Production over Pd Nanoparticles Decorated with g-C_3N_5 Photocatalyst

Trinh Duy Nguyen [1,*], Nhat Le-Duy [1], Que-Minh T. Doan [2], Lan-Anh T. Hoang [1] and Taeyoon Lee [1,*]

[1] Department of Environmental Engineering, College of Environmental and Marine Sciences and Technology, Pukyong National University, 45 Yongso-ro, Nam-gu, Busan 48513, Republic of Korea; nhatleduy.16@gmail.com (N.L.-D.); anhhtl5nk@wru.vn (L.-A.T.H.)

[2] Institute of Applied Technology and Sustainable Development, Nguyen Tat Thanh University, Ho Chi Minh City 700000, Vietnam; dtqminh@ntt.edu.vn

* Correspondence: ndtrinh@ntt.edu.vn (T.D.N.); badger74w@pknu.ac.kr (T.L.)

Abstract: A uniform distribution of Pd nanoparticles on g-C_3N_5 layers is achieved through wet-chemical reduction (Pd/g-C_3N_5-EG). Pd/g-C_3N_5-EG demonstrates superior hydrogen production yield compared to heterojunctions synthesized via photoreduction (Pd/g-C_3N_5-PR), attributed to improved metal–support interaction. Pd/g-C_3N_5-EG demonstrates an average hydrogen evolution rate of 891.304 μmol g^{-1} h^{-1}, representing a 7.8-fold increase over Pd/g-C_3N_5-PR and a 34.5-fold increase over bare g-C_3N_5. Pd/g-C_3N_5-EG also maintains its hydrogen production capability after five recycling cycles, with only a slight decrease in efficiency.

Keywords: hydrogen production; Pd nanoparticles; g-C_3N_5 photocatalyst; heterojunction

1. Introduction

Nitrogen-rich carbon nitride g-C_3N_5 recently received much attention as a newly emerged photocatalyst. In comparison to g-C_3N_4, g-C_3N_5 exhibits a narrower band gap energy and a higher potential of having a conductive band (CB) due to the nitrogen-rich matrix. In particular, the presence of a triazole unit with N–N coupling within the g-C_3N_5 framework enhances its ability to absorb light, extending its absorption range into the visible spectrum—substantially broader than that of g-C_3N_4 [1,2]. As a result, g-C_3N_5 has been increasingly considered as a viable alternative to g-C_3N_4 in various applications, including photocatalytic degradation of organic compounds [3] and H_2 production [4]. However, similar to single-component photocatalysts, sluggish charge transfer may hinder its broader application. The synthesis of composites containing g-C_3N_5 and metallic/bimetallic nanoparticles could provide a versatile approach to enhancing the H_2 evolution of g-C_3N_5 [5]. Under irradiation, electrons in the valence band (VB) of g-C_3N_5 undergo excitation, moving to the CB of g-C_3N_5 and leaving behind a hole in the VB of g-C_3N_5. The efficient electron/hole separation is preferably achieved when metallic/bimetallic nanoparticles are anchored on a g-C_3N_5 server as electron acceptors. Electron acceptors play a crucial role in capturing electrons from the CB of g-C_3N_5, thereby initiating the hydrogen evolution reaction on the conduction band of g-C_3N_5 layers. During this process, protons (H^+) react with captured electrons to produce H_2, attributed to the more positive CB value of g-C_3N_5 in comparison to the standard reduction potential (H^+/H_2).

The distribution and loading of metallic/bimetallic nanoparticles on the g-C_3N_5 layers has been achieved through various methods, such as wet-chemical reduction, photochemical reduction, and high-temperature reduction under an inert atmosphere. Among these,

check for updates

Academic Editors: Maria Victoria López Ramón and Mariana de Mattos V. M. Souza

Received: 27 November 2024
Revised: 5 January 2025
Accepted: 10 January 2025
Published: 15 January 2025

Citation: Nguyen, T.D.; Le-Duy, N.; Doan, Q.-M.T.; Hoang, L.-A.T.; Lee, T. Improving Photocatalytic Hydrogen Production over Pd Nanoparticles Decorated with g-C_3N_5 Photocatalyst. *Processes* **2025**, *13*, 235. https://doi.org/10.3390/pr13010235

Copyright: © 2025 by the authors. Licensee MDPI, Basel, Switzerland. This article is an open access article distributed under the terms and conditions of the Creative Commons Attribution (CC BY) license (https://creativecommons.org/licenses/by/4.0/).

the wet-chemical reduction method using organic capping ligands enables the controllable size and uniform distribution of metallic and bimetallic nanoparticles on g-C_3N_5 layers, which is expected to significantly enhance photocatalytic activity compared to other synthesis methods [6,7].

In our approach, we employ wet-chemical reduction using ethylene glycol (EG) acting as both a capping and reduction agent for loading Pd° nanoparticles (NPs) on the g-C_3N_5 matrix, ensuring a better metal–support interaction. For comparison, we also synthesized Pd/g-C_3N_5 via the photoreduction method. In addition, the Pd/g-C_3N_5 composite, prepared according to these methods and employing $PdCl_2$ as the Pd source, may be more cost-effective than using Pt. This approach avoids the introduction of additional impurities, allows for easy control of the reaction conditions, maintains a low production cost, and facilitates straightforward large-scale production.

2. Materials and Methods

2.1. Materials

All the chemicals were used without further purification. 3-amino-1,2,4-triazole ($C_2H_4N_4$, 99%), palladium (II) chloride ($PdCl_2$, 99%), and Nafion (5 wt.% in lower aliphatic alcohols and water, contains 45% water) were purchased from Sigma-Aldrich (St. Louis, MO, USA). Ethylene glycol (EG, $C_2H_6O_2$, 99%), methanol (CH_4O, 99%), ethanol (C_2H_6O, 99%), potassium ferricyanide ($K_3Fe(CN)_6$, 99%), sodium sulfate (Na_2SO_4, 99%), potassium cyanide (KCN, 98%), and triethanolamine (TEOA, $C_6H_{15}NO_3$, 99%) were purchased from Junsei (Tolyo, Japan).

2.2. Synthesis of g-C_3N_5 Photocatalyst by a Thermal Condensation Method

The g-C_3N_5 photocatalyst was fabricated using a thermal condensation method with 3-amino-1,2,4-triazole as the starting material [8]. Specifically, 3 g of 3-amino-1,2,4-triazole powder was thoroughly ground into an aluminum crucible with a lid. The crucible was then heated to 550 °C in a muffle furnace for 4 h under ambient conditions, with a heating rate of 5 °C min^{-1}. The as-obtained sample was ground into a fine powder, and after dispersing deionized water, it was stirred continuously for 2 h. The final g-C_3N_5 sample was collected by centrifuge and dried under vacuum at 60 °C overnight.

2.3. Synthesis of Pd/g-C_3N_5 Composite

The Pd/g-C_3N_5 heterojunction was synthesized by the wet-chemical method, referred to as Pd/g-C_3N_5-EG. In a typical procedure, 300 mg of g-C_3N_5 was dissolved in 100 mL of EG, sonicated for 30 min, and then placed in the ice-water bath with continuous stirring. After stirring for 30 min, 0.6 mL of $PdCl_2$ solution (2.5 mg Pd/mL) was added dropwise into the g-C_3N_5-EG suspension, followed by additional stirring for 2 h. The Pd content was set at 0.5 wt.%. Then, the solution was transferred into a flask and heated in an oil bath at 140 °C for 2 h. After cooling to room temperature, the Pd/g-C_3N_5-EG solid was collected by centrifugation, washed with deionized water and ethanol at least three times, and finally dried under vacuum overnight at 60 °C.

For comparison, the Pd/g-C_3N_5 composite was also synthesized via a photoreduction method, denoted as Pd/g-C_3N_5-PR. Firstly, 300 mg of g-C_3N_5 was suspended, dispersed in 100 mL of 20% (*v*/*v*) methanol solution, and sonicated for 30 min to form a suspension. Then, the mixture was transferred into the double-layer beaker, and 0.6 mL of $PdCl_2$ solution (2.5 mg mL^{-1}) was added dropwise to the suspension. The Pd content was set at 0.5 wt.%. The suspension was stirred for the next 2 h before it was illuminated under a 300 W Xenon lamp with a 420 nm filter cutoff for 2 h. The Pd/g-C_3N_5-PR product was collected by centrifuge, rinsed with ethanol and DI water several times, and dried at 60 °C overnight.

2.4. Characterization

The crystal structure of photocatalysts was analyzed using X-ray diffraction (XRD) spectra from an X'Pert3-Powder X-Ray Diffractometer (PANalytical, Malvern, UK) with a 2θ range of 10–80°. The morphologies and structures of as-prepared catalysts were investigated by field emission transmission electron microscopy (FE-TEM) and energy-dispersive spectroscopy (EDS, Tokyo, Japan) analysis using JEM-F200 (JEOL, Tokyo, Japan). UV-Vis diffuse reflection spectra (UV-Vis DRS) of g-C_3N_5 and Pd/g-C_3N_5 photocatalysts were recorded using Shimadzu UV-Vis spectroscopy (UV-2600, Tokyo, Japan). The photoluminescence (PL) spectra of the as-prepared samples were obtained at room temperature using a photofluorescence luminescence spectrophotometer system (Fluorolog-QM, HORIBA, Kyoto, Japan), with the excitation wavelength set at 360 nm.

2.5. Electrochemical Analysis

The electrochemical measurements were performed using a ZIVELAB single-channel electrochemical workstation (Seoul, Republic of Korea). The Ag/AgCl electrode, Pt wire, and ITO substance with the sample were used as the reference, counter, and working electrodes, respectively, for the three-electrode system. The working electrodes were prepared as follows: the as-prepared photocatalyst (10 mg) was mixed with a solution containing 20 μL Nafion and 1 mL isopropanol solution (isopropanol/H_2O = 1/3 v/v). Then, the mixture was sonicated for 60 min before being coated on an ITO glass (5 mm × 15 mm). Electrochemical impedance spectroscopy (EIS) Nyquist was performed with the frequency set in the range of 0.1 Hz to 1 MHz and an amplitude of 5 mV. The electrolyte solution was a mixture of $K_3Fe(CN)_6$ and KCN at concentrations of 2 mM and 1 M, respectively. The Mott–Schottky test was performed at a frequency of 1 kHz, and the amplitude was in the range of −1 V and 1 V, using 0.5 M of Na_2SO_4 (pH = 6.97) as the electrolyte. Electrochemical measurements were performed in the dark. The data were analyzed using ZMAN 2.5 software.

2.6. Catalytic Activity Tests

The photocatalytic activity of the as-synthesized samples was evaluated by measuring their efficiency of H_2 production. In brief, 50 mg of the photocatalyst was evenly dispersed in 10 mL of TEOA and 90 mL of DI water through sonication. This mixture was then transferred to a 250 mL flask, which was sealed with a rubber stopper. The gas was removed by vacuuming for 15 min, followed by N_2 gas purging for an additional 15 min. After that, the flask was illuminated with a 300 W Xenon lamp with the 420 nm cutoff filter for 3 h to facilitate H_2 production. The generated H_2 gas was determined using an HP gas chromatograph (GC5890 series II, Santa Clara, CA, USA) equipped with a thermal conductivity detector (TCD), using 5 Å molecular sieve columns and Ar as the carrier gas. The calibration of the TCD signal for H_2 using various dilutions of H_2 in N_2 is shown in Figure 1. To confirm the stability of the photocatalyst, a recycling test was conducted. The catalyst was washed with ethanol and DI water after each cycle, and their photocatalytic performance was re-evaluated.

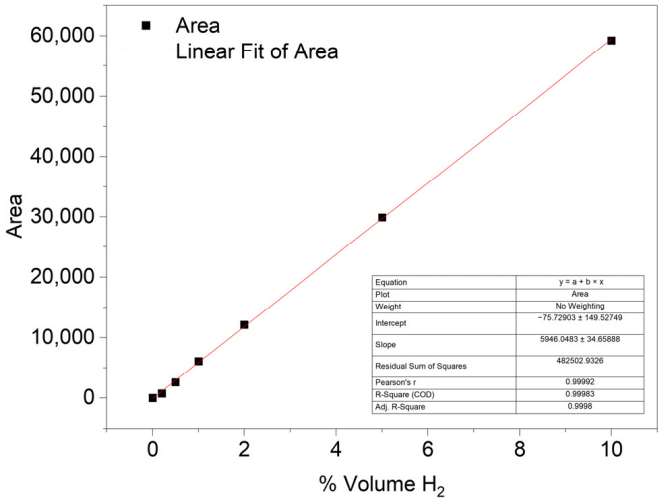


Figure 1. The calibration of the TCD signal for H_2 using various dilutions of H_2 in N_2.

3. Results

The Pd/g-C_3N_5 composites were prepared following the procedure outlined in Figure 2. Initially, g-C_3N_5 was synthesized by heating 3-amino-1,2,4-triazole at 550 °C under an ambient atmosphere. Subsequently, the wet-chemical reduction and photoreduction methods were applied to distribute metallic Pd nanoparticles onto the g-C_3N_5 layer. In both routers, a $PdCl_2$ solution served as the precursor solution to form the metallic Pd nanoparticles. In the wet-chemical reduction, the Pd^{2+} ion in the solution was reduced to Pd by EG. In the photoreduction method, the Pd^{2+} ion in the solution was reduced to Pd by the electrons from the conduction band of g-C_3N_5 during the photocatalytic reaction. In addition, the presence of EG as an organic capping ligand facilitates precise control over the shape and size of Pd nanoparticles, which is expected to enhance their photocatalytic activity.

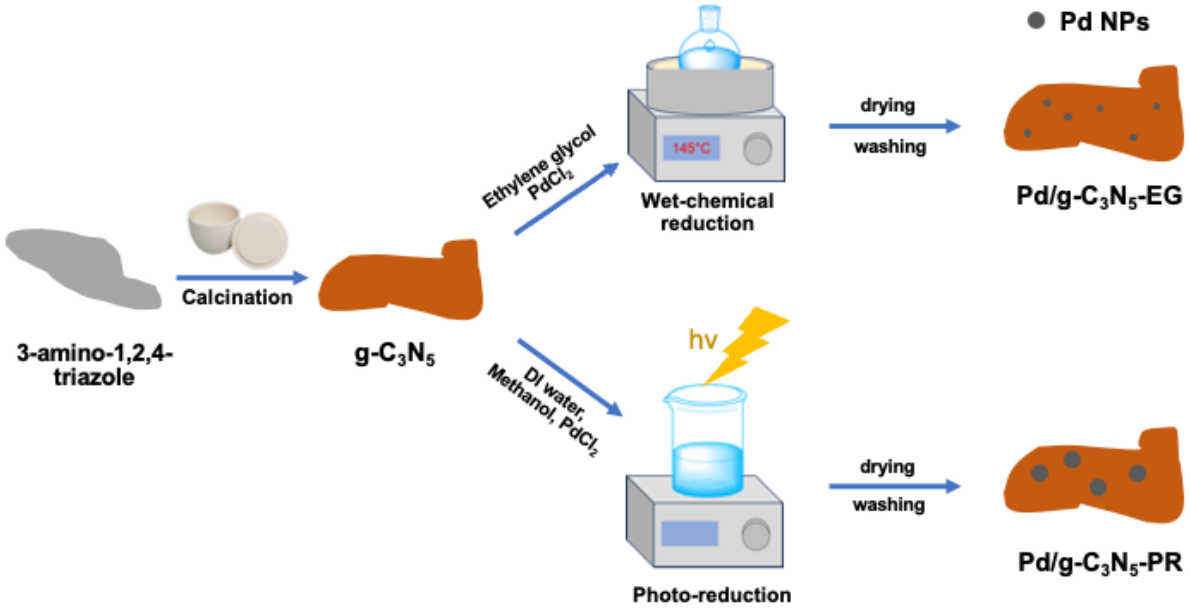


Figure 2. Schematic illustration of the preparation of g-C_3N_5 and Pd/g-C_3N_5 composites.

The XRD patterns of all catalysts are consistent with those reported in previous studies on g-C_3N_5 (Figure 3A) [1,9]. The introduction of metallic Pd does not appear to significantly alter the crystalline structure of g-C_3N_5. Additionally, the distinct peaks of the Pd° NPs

were not observed, due to the tiny atomic diameter of metallic Pd° nanoparticles and their relatively low concentration in the composite. Pd° and Pd^{2+} species were detected in both Pd/g-C_3N_5-EG and Pd/g-C_3N_5-PR samples (Figure 3B). Notably, the Pd° content was highest in Pd/g-C_3N_5-EG, indicating that the wet-chemical reduction method employing EG as a reducing agent was particularly effective in promoting Pd^{2+} reduction. In addition, compared to g-C_3N_5-PR (Figure 3(C1,C2)), Pd/g-C_3N_5-EG (Figure 3(D1,D2)) shows a finely dispersed metallic Pd homogeneously distributed on g-C_3N_5 layers, underscoring the superiority of the wet-chemical reduction method for synthesizing metallic Pd over the photoreduction method. This outcome is anticipated to result in enhanced photoelectrochemical properties.

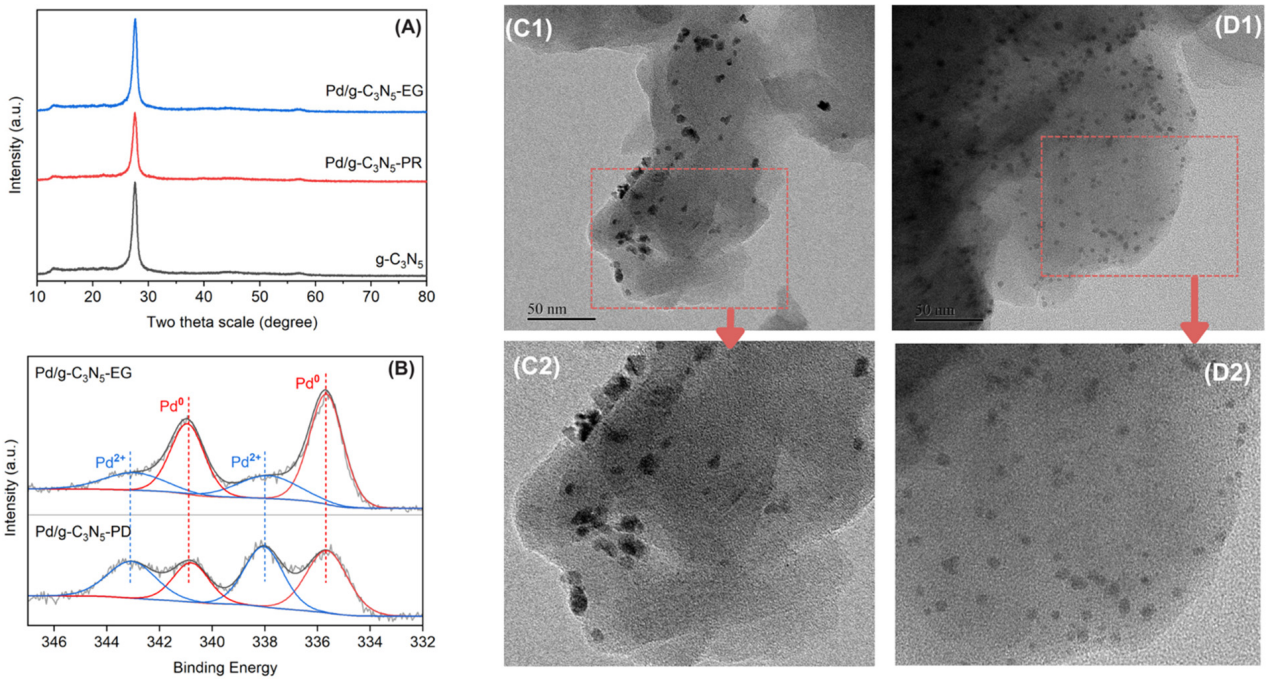


Figure 3. XRD of g-C_3N_5 and Pd/g-C_3N_5 composites (**A**); high-resolution XPS of Pd 3d (**B**); TEM images of Pd/g-C_3N_5-PR (**C1**,**C2**); and Pd/g-C_3N_5-EG (**D1**,**D2**).

Figure 4 illustrates the N_2 adsorption–desorption isotherms and pore width distribution for catalysts. The g-C_3N_5 possesses a BET surface area of 12 m^2 g^{-1} with a pore size of 4 to 6 nm. The introduction of Pd° NPs in g-C_3N_5 did not significantly change the textural properties of the g-C_3N_5.

Figure 5A depicts the ultraviolet–visible diffuse reflectance spectra of pure and Pd°-decorated g-C_3N_5 samples. The g-C_3N_5 exhibits robust absorption across the solar spectrum, with a band edge wavelength of 650 nm, which is attributed to its narrow band gap [1,5,9]. The absorption spectra of g Pd/g-C_3N_5 composites appear to undergo no significant change upon the introduction of metallic Pd. The band gap (E_g) values for pure and Pd°-decorated g-C_3N_5 samples were determined from the plots of $(\alpha h\nu)^{1/2}$ against photon energy (Figure 5B). The estimated E_g values were 1.95 eV for g-C_3N_5, 1.87 eV for Pd/g-C_3N_5-EG, and 1.91 eV for Pd/g-C_3N_5-PR.

Figure 5C illustrates the photoluminescence of g-C_3N_5 and Pd/g-C_3N_5 composites. The g-C_3N_5 samples exhibit an emission peak in the range of 400–600 nm, which is attributed to the band-to-band photoluminescence [1]. The Pd/g-C_3N_5 composites show a lower photoluminescence intensity compared to g-C_3N_5, indicating that the recombination rate has been effectively suppressed due to the introduction of Pd° NPs.

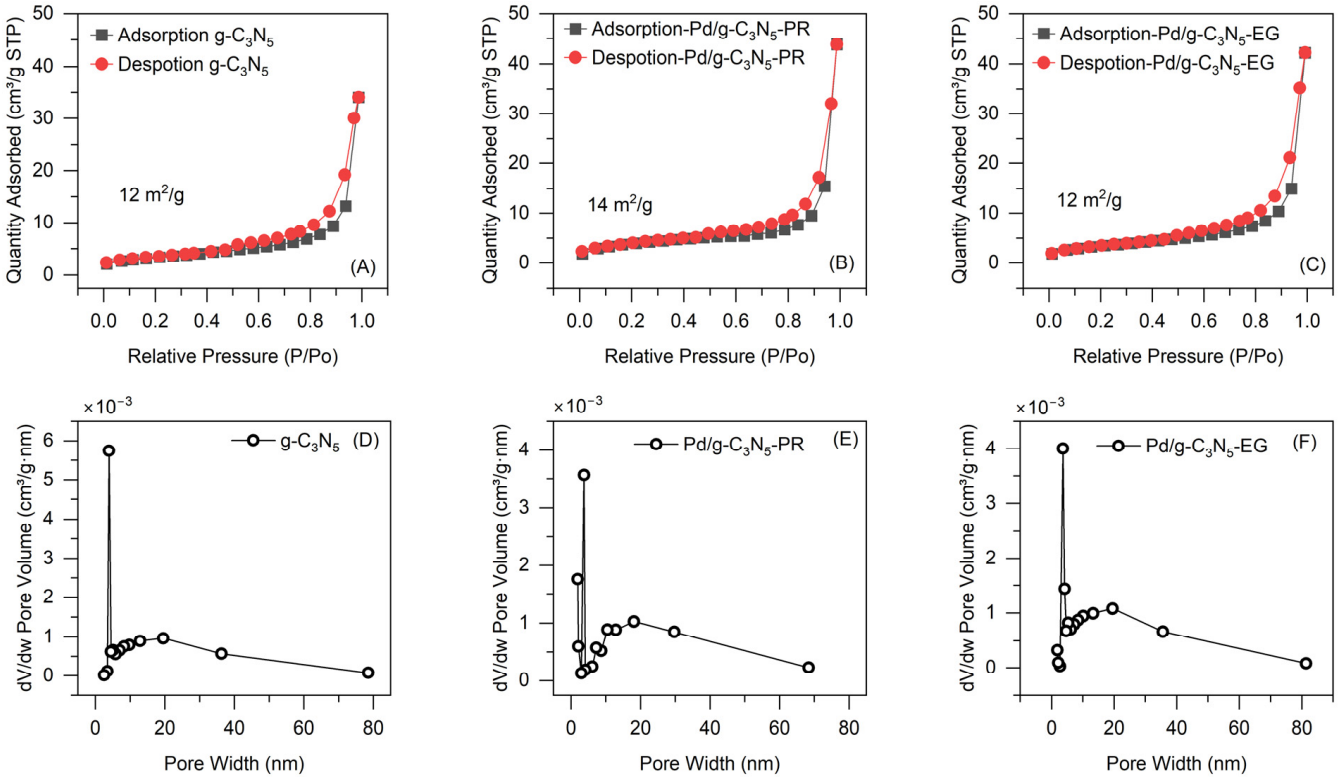


Figure 4. N_2 adsorption–desorption isotherms of g-C_3N_5 (**A**), Pd/g-C_3N_5-PR (**B**), and Pd/g-C_3N_5-EG (**C**), and the pore-size distribution curves of g-C_3N_5 (**D**), Pd/g-C_3N_5-PR (**E**), and Pd/g-C_3N_5-EG (**F**).

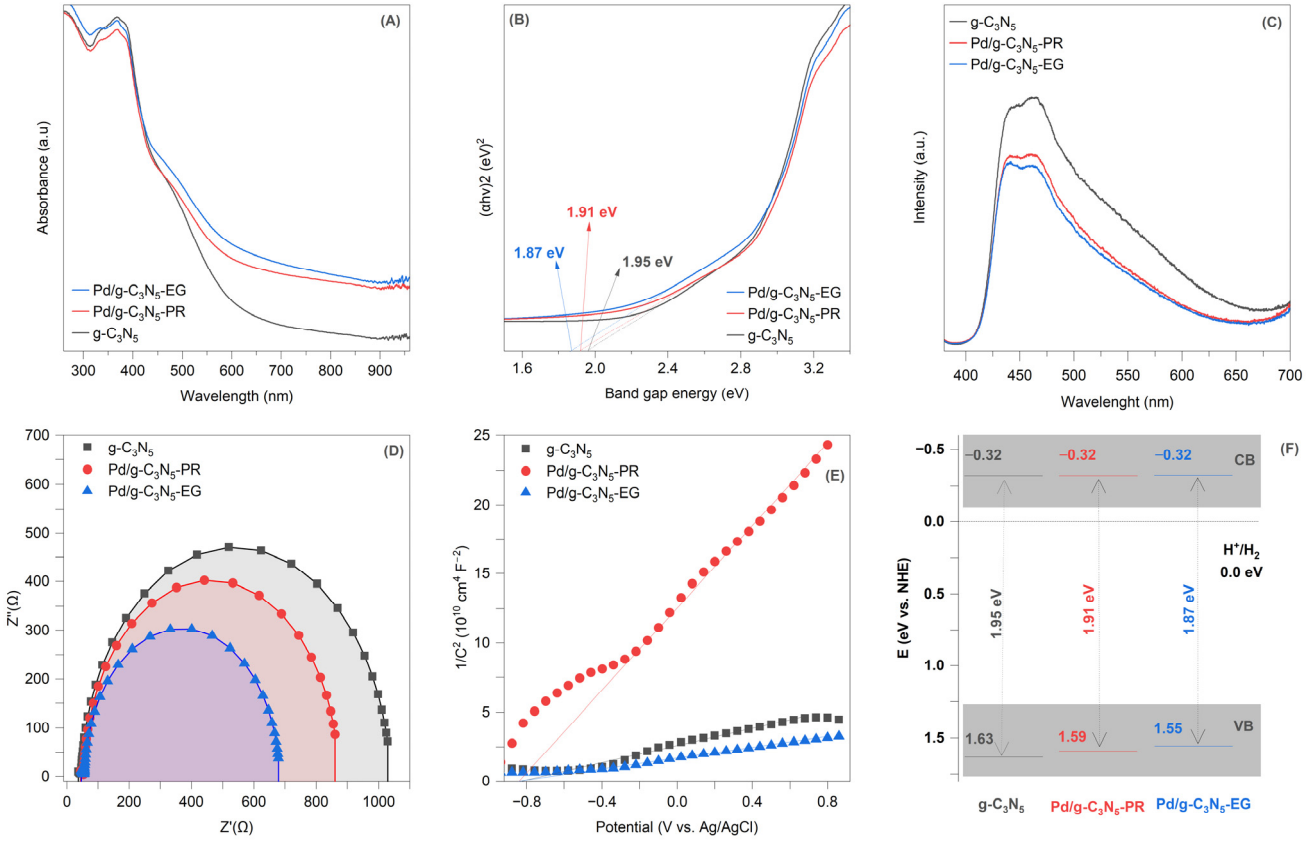


Figure 5. Ultraviolet–visible diffuse reflectance spectra (**A**); plots of $(\alpha h\nu)^{1/2}$ against photon energy (**B**); photoluminescence (**C**); Nyquist plots (**D**); Mott–Schottky plots (**E**); and schematic energy band diagram (**F**) of pure and Pd°-decorated g-C_3N_5 samples.

In the Nyquist plot, a higher curvature corresponds to lower charge transfer resistance. The curvature of the Nyquist curve follows the order of Pd/g-C_3N_5-EG > Pd/g-C_3N_5-PR > g-C_3N_5, indicating that Pd/g-C_3N_5-EG has the smallest impedance (Figure 5D). This finding verifies the improved charge transfer mechanism at the interface between Pd° NPs and g-C_3N_5, facilitating the movement of charge carriers. The excellent electron transport efficiency from g-C_3N_5 to Pd° NPs enhances the transmission and separation of charge carriers, thereby improving photocatalytic hydrogen production performance. Moreover, the Pd° NP-decorated g-C_3N_5 layer synthesized via wet-chemical reduction demonstrated a more effective metal–support interaction compared to the photoreduction method, leading to an expected higher hydrogen production yield. As discussed in the introduction section, the wet-chemical reduction method, employing organic capping ligands, facilitates the precise control of nanoparticle size and ensures a uniform distribution of Pd° NPs on g-C_3N_5 layers. This approach is anticipated to significantly affect the interface properties between Pd° NPs and g-C_3N_5 compared to the photoreduction method.

The conduction band level (E_{CB}) was determined using Mott–Schottky plots (Figure 5E). The E_{CB} values for all samples were determined to be −0.32 eV (vs. NHE), as previously demonstrated [10]. The valence band position (E_{VB}) was then calculated using the following equation: $Eg = E_{VB} - E_{CB}$. Based on this, the E_{VB} values are 1.55 eV for Pd/g-C_3N_5-EG, 1.59 eV for Pd/g-C_3N_5-PR, and 1.63 eV for g-C_3N_5. The energy band diagrams for pure and Pd°-decorated g-C_3N_5 samples are illustrated in Figure 5F.

Figure 6A shows the photocatalytic H_2 evolution rates over g-C_3N_5 and Pd/g-C_3N_5 composites. The average hydrogen evolution rate for Pd/g-C_3N_5-EG is approximately 891.304 μmol g^{-1} h^{-1} under visible light irradiation, representing a 34.5-fold increase compared to the pristine g-C_3N_5 at 23.753 μmol g^{-1} h^{-1} and a 7.8-fold increase compared to Pd/g-C_3N_5-PR at 113.418 μmol g^{-1} h^{-1}. Figure 6B shows photocatalytic H_2 evolution rates over Pd/g-C_3N_5-EG composites after five reaction cycles. The hydrogen evolution performances of Pd/g-C_3N_5-EG remain stable across the testing cycles, highlighting the excellent stability of the catalysts.

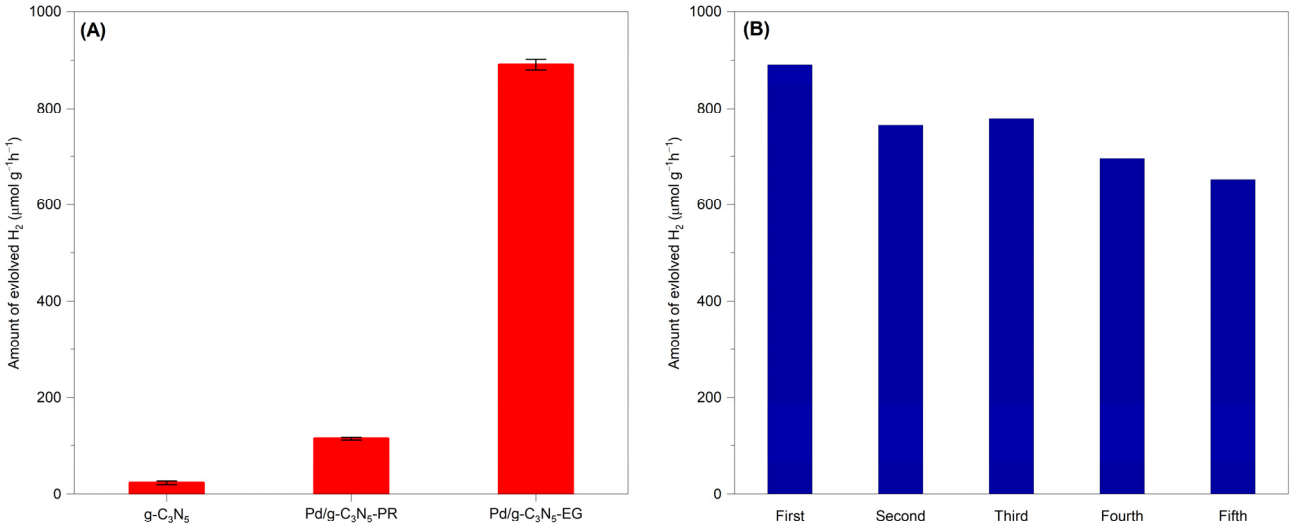


Figure 6. Photocatalytic H_2 evolution rates over g-C_3N_5 and Pd/g-C_3N_5 composites (**A**); photocatalytic H_2 evolution rates over Pd/g-C_3N_5-EG composites after five reaction cycles (**B**).

The schematic band structure diagram of g-C_3N_5 and Pd/g-C_3N_5 composites (Figure 5F) reveals minimal differences in the CB and VB values between g-C_3N_5 and Pd/g-C_3N_5, suggesting the establishment of the heterojunction between Pd° NPs and the g-C_3N_5 layer. In this configuration, Pd° NPs play a role as electron traps, accumulating

electrons from g-C_3N_5 due to the smaller work function of g-C_3N_5 (5.2 eV vs. vacuum [11]) compared to Pd° (5.6 eV vs. vacuum [12]). The establishment of a heterojunction effectively prevents the reverse migration of electrons trapped by Pd° NPs, thus promoting enhanced electron-transfer pathways. In addition, the Pd nanoparticle-decorated g-C_3N_5 layer, obtained through wet-chemical reduction, exhibited an excellent hydrogen production yield compared to the Pd° nanoparticle-decorated g-C_3N_5 layer obtained by photoreduction. The smaller size and uniform distribution of Pd° NPs in the wet-chemical reduction process can enhance the effective metal–support interaction with g-C_3N_5 layers. As a result, the favorable electronic transmission properties of uniformly distributed Pd° NPs in the Pd/g-C_3N_5-EG enable them to act as electron acceptors, effectively capturing photogenerated electrons and accelerating the separation of electron–hole pairs, thereby enhancing hydrogen production yield.

Because the energy level of the photogenerated electrons on the CB of g-C_3N_5 (−0.32 eV) is higher than the H^+/H_2 redox level (0.0 eV), these electrons produced by g-C_3N_5 under visible light irradiation can effectively reduce H^+ to generate H_2. However, the presence of O_2 and photogenerated holes can hinder the H_2 evolution process. To mitigate their effects, O_2 was purged from the reactor using N_2 gas and the holes were trapped by triethanolamine (TEOA). In this inert atmosphere, the H_2 evolution process can be described by Equations (1)–(3).

$$g - C_3N_5 \xrightarrow{h\theta} e^- + h^+ \quad (1)$$

$$H^+ + 2e^- \rightarrow \frac{1}{2}H_2 \quad (2)$$

$$TEOA + h^+ \rightarrow TEOA^+ \quad (3)$$

However, the rapid recombination of photogenerated carriers may limit the photocatalytic activity of g-C_3N_5. To overcome this, Pd° NPs, acting as electron accepters, can capture the photogenerated electrons from the CB of g-C_3N_5. Then, these electrons migrate to the Pd° NP surface, where they participate in the reduction of H^+ to generate H_2.

4. Conclusions

We have successfully synthesized Pd° NPs decorated on the Pd/g-C_3N_5 layers using two methods: (1) wet-chemical reduction with EG serving as both a capping and reduction agent and (2) a photoreduction method employing a 10% v/v methanol solution under irradiation of a 300 Xenon light lamp. The results indicated that Pd/g-C_3N_5 synthesized via wet-chemical reduction exhibited enhanced optical and electrochemical properties compared to Pd/g-C_3N_5 obtained by the photoreduction method. This improvement is due to the wet-chemical reduction method, which facilitates the uniform deposition of Pd° NPs and promotes a more effective metal–support interaction, highlighting the superiority of the wet-chemical reduction method over the photoreduction method for synthesizing Pd° NPs. As a result, the Pd NP-decorated g-C_3N_5 layer, obtained through wet-chemical reduction, exhibited an excellent H_2 production yield compared to heterojunctions obtained by photoreduction. In addition, the performance of the Pd/g-C_3N_5 material for hydrogen production was evaluated over five recycling cycles. Although a slight decrease in hydrogen after five recycling cycles may be attributed to the loss of catalysts, the photocatalyst maintained its utility for sustained hydrogen production. Our study presents an approach that enables easy control of reaction conditions, maintains a low production cost, and facilitates the straightforward large-scale synthesis of metal–photocatalyst heterojunctions to improve H_2 production.

Author Contributions: T.D.N.: writing—original draft, data curation, methodology, visualization. N.L.-D.: data curation, methodology. Q.-M.T.D.: data curation, methodology. L.-A.T.H.: data curation, methodology. T.L.: writing—review and editing, methodology, visualization, supervision. All authors have read and agreed to the published version of the manuscript.

Funding: This research was supported by the Pukyong National University Industry-university Cooperation Foundation's 2024 Post-Doc. support project.

Data Availability Statement: The original contributions presented in the study are included in the article; further inquiries can be directed to the corresponding author.

Conflicts of Interest: The authors declare no conflicts of interest.

References

1. Kumar, P.; Vahidzadeh, E.; Thakur, U.K.; Kar, P.; Alam, K.M.; Goswami, A.; Mahdi, N.; Cui, K.; Bernard, G.M.; Michaelis, V.K.; et al. C_3N_5: A Low Bandgap Semiconductor Containing an Azo-Linked Carbon Nitride Framework for Photocatalytic, Photovoltaic and Adsorbent Applications. *J. Am. Chem. Soc.* **2019**, *141*, 5415–5436. [CrossRef] [PubMed]
2. Kim, I.Y.; Kim, S.; Jin, X.; Premkumar, S.; Chandra, G.; Lee, N.; Mane, G.P.; Hwang, S.; Umapathy, S.; Vinu, A. Ordered Mesoporous C_3N_5 with a Combined Triazole and Triazine Framework and Its Graphene Hybrids for the Oxygen Reduction Reaction (ORR). *Angew. Chem. Int. Ed.* **2018**, *57*, 17135–17140. [CrossRef] [PubMed]
3. Fu, C.; Zhao, M.; Chen, X.; Sun, G.; Wang, C.; Song, Q. Unraveling the dual defect effects in C_3N_5 for piezo-photocatalytic degradation and H_2O_2 generation. *Appl. Catal. B* **2023**, *332*, 122752. [CrossRef]
4. Liu, H.; Hu, J.; Sun, C.; Wu, L.; Jiao, F. Insight into the key role of proton-functionalization in metal-free C_3N_5 activated visible light system for efficient hydrogen evolution reaction. *Int. J. Hydrogen Energy* **2024**, *59*, 306–315. [CrossRef]
5. Du, X.; Liu, Q.; Cheng, M.; Wang, R.; Hu, J.; Wei, T.; Ling, Y.; Cui, Y.; Li, W.; Liu, B. Single-atom Pt decorated g-C_3N_5 nanorods as highly efficient photocatalyst for H_2 evolution and wastewater purification. *Int. J. Hydrogen Energy* **2024**, *53*, 353–363. [CrossRef]
6. Liu, Y.; Du, C.; Zhou, C.; Yang, S. One-step synthesis of hierarchical AuNPs/$Cd_{0.5}Zn_{0.5}S$ nanoarchitectures and their application as an efficient photocatalyst for hydrogen production. *J. Ind. Eng. Chem.* **2019**, *72*, 338–345. [CrossRef]
7. Ding, D.; Liu, K.; He, S.; Gao, C.; Yin, Y. Ligand-exchange assisted formation of Au/TiO_2 Schottky contact for visible-light photocatalysis. *Nano Lett.* **2014**, *14*, 6731–6736. [CrossRef] [PubMed]
8. Mane, G.P.; Talapaneni, S.N.; Lakhi, K.S.; Ilbeygi, H.; Ravon, U.; Al-Bahily, K.; Mori, T.; Park, D.; Vinu, A. Highly Ordered Nitrogen-Rich Mesoporous Carbon Nitrides and Their Superior Performance for Sensing and Photocatalytic Hydrogen Generation. *Angew. Chem. Int. Ed.* **2017**, *56*, 8481–8485. [CrossRef] [PubMed]
9. Wang, H.; Li, M.; Lu, Q.; Cen, Y.; Zhang, Y.; Yao, S. A Mesoporous Rod-like g-C_3N_5 Synthesized by Salt-Guided Strategy: As a Superior Photocatalyst for Degradation of Organic Pollutant. *ACS Sustain. Chem. Eng.* **2019**, *7*, 625–631. [CrossRef]
10. Che, H.; Wang, J.; Gao, X.; Chen, J.; Wang, P.; Liu, B.; Ao, Y. Regulating directional transfer of electrons on polymeric g-C_3N_5 for highly efficient photocatalytic H_2O_2 production. *J. Colloid Interface Sci.* **2022**, *627*, 739–748. [CrossRef] [PubMed]
11. Yang, H.; Li, W.; Jiang, Y.; Wei, Q.; Hou, L.; Wu, Z.; He, Q.; Wang, Y.; Tang, D. Diethylenetriamine-CdS hybrid materials (CdS-DETA) loaded nitrogen-rich carbon nitride (g-C_3N_5) for enhanced hydrogen production and photocatalytic degradation: Enhancement based on band bending. *Sep. Purif. Technol.* **2023**, *304*, 122375. [CrossRef]
12. Kang, J.; Liu, W.; Sarkar, D.; Jena, D.; Banerjee, K. Computational Study of Metal Contacts to Monolayer Transition-Metal Dichalcogenide Semiconductors. *Phys. Rev. X* **2014**, *4*, 031005. [CrossRef]

Disclaimer/Publisher's Note: The statements, opinions and data contained in all publications are solely those of the individual author(s) and contributor(s) and not of MDPI and/or the editor(s). MDPI and/or the editor(s) disclaim responsibility for any injury to people or property resulting from any ideas, methods, instructions or products referred to in the content.